Supplemental Section A. Histology of tissue at the edge of the ECoG grid

Fluorescence microscopy was used to assess the transition area between the edge of ECoG grid and the tissue immediately adjacent to the device (Supplemental Figure A1). We observed anatomical continuity in the transition area, with limited changes in neuron (red) and microglia (green) populations as well as the cortical layer structure.

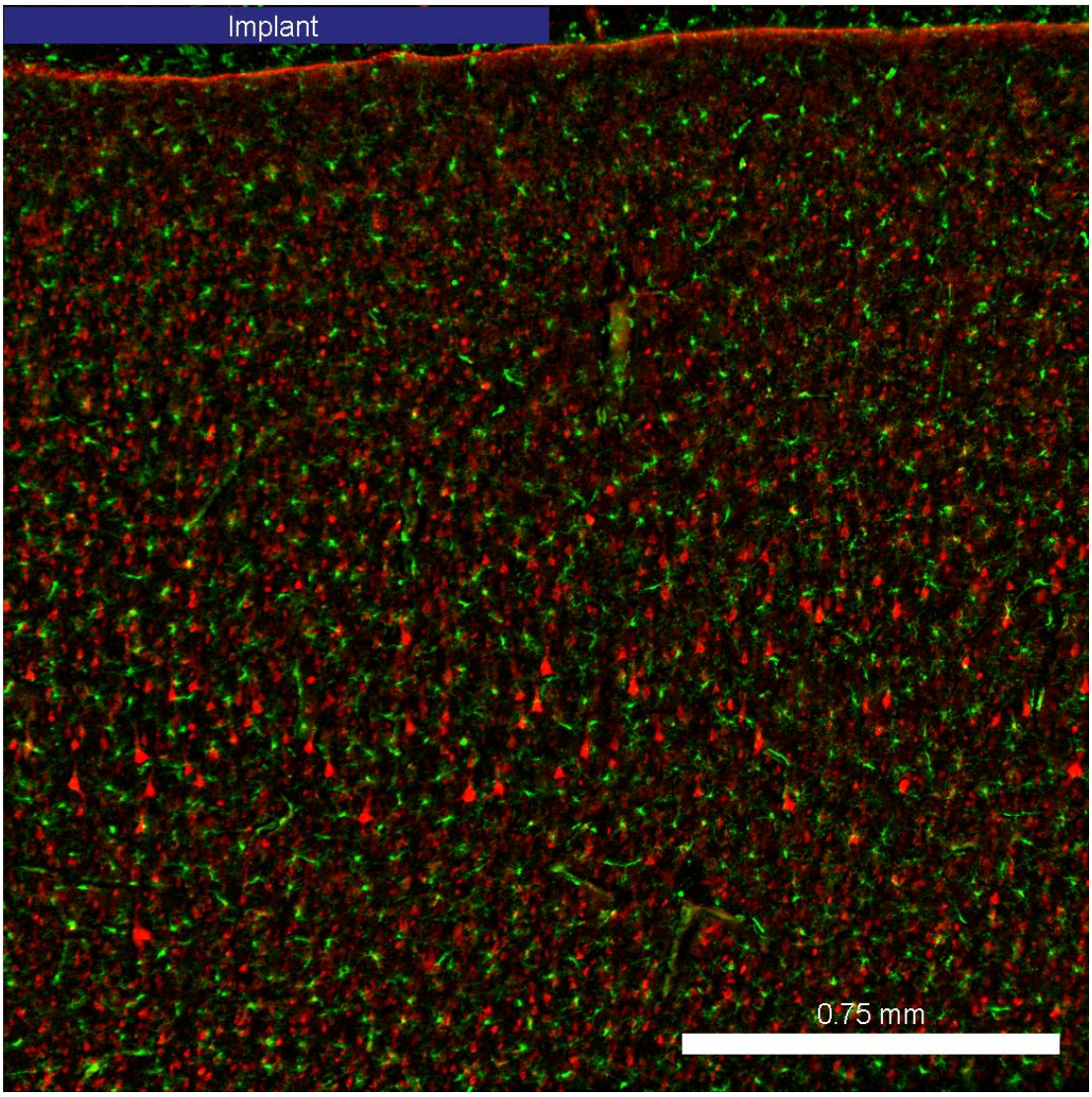

Supplemental Figure A1. Fluorescence microscopy of neural tissue under the edge of the ECoG array (blue box) and the adjacent tissue. No observable changes in cortical architecture as determined by neuronal morphology (red). Microglia in green.

Supplemental Section B. ECoG modulation during overt arm movements

In order to assess the functional properties of ECoG signals recorded during the center-out reaching task, ECoG signals were fit to a standard cosine tuning model (Georgopoulos et al., 1982). Normalized spectral data was first averaged over the [70 - 110] Hz frequency band over the [-100ms , 100ms] interval relative to movement onset for each trial. Cosine tuning curves were fit to this averaged data using equation B.1:

$$f = b_0 + b_x x + b_y y + \varepsilon \qquad \text{(B.1)}$$

Supplemental Figure B1 shows normalized spectral data for each target and electrode during center-out hand control trials. Despite differences in electrode position on the cortex, nearly all electrodes show preferential modulation for upper-left targets. This is confirmed by the results of the cosine tuning analysis shown in Supplemental Figure B2. The preferred directions of high-gamma band activity from all electrodes were tightly clustered during the center-out task, as would be expected from the highly correlated time-frequency data shown by Figure 5 and Supplemental Figure B1. It is unclear what role the fibrotic encapsulation observed upon explantation of the electrode grid may have played in the observed inter-electrode correlation. It is possible that the increased distance between the electrodes and the cortex resulting from the growth of the encapsulation tissue may have resulted in an increase in inter-electrode correlation. Additional studies are required in order to better understand how the functional specificity of ECoG signals recorded from motor cortex varies as electrodes are moved further from the cortical surface.

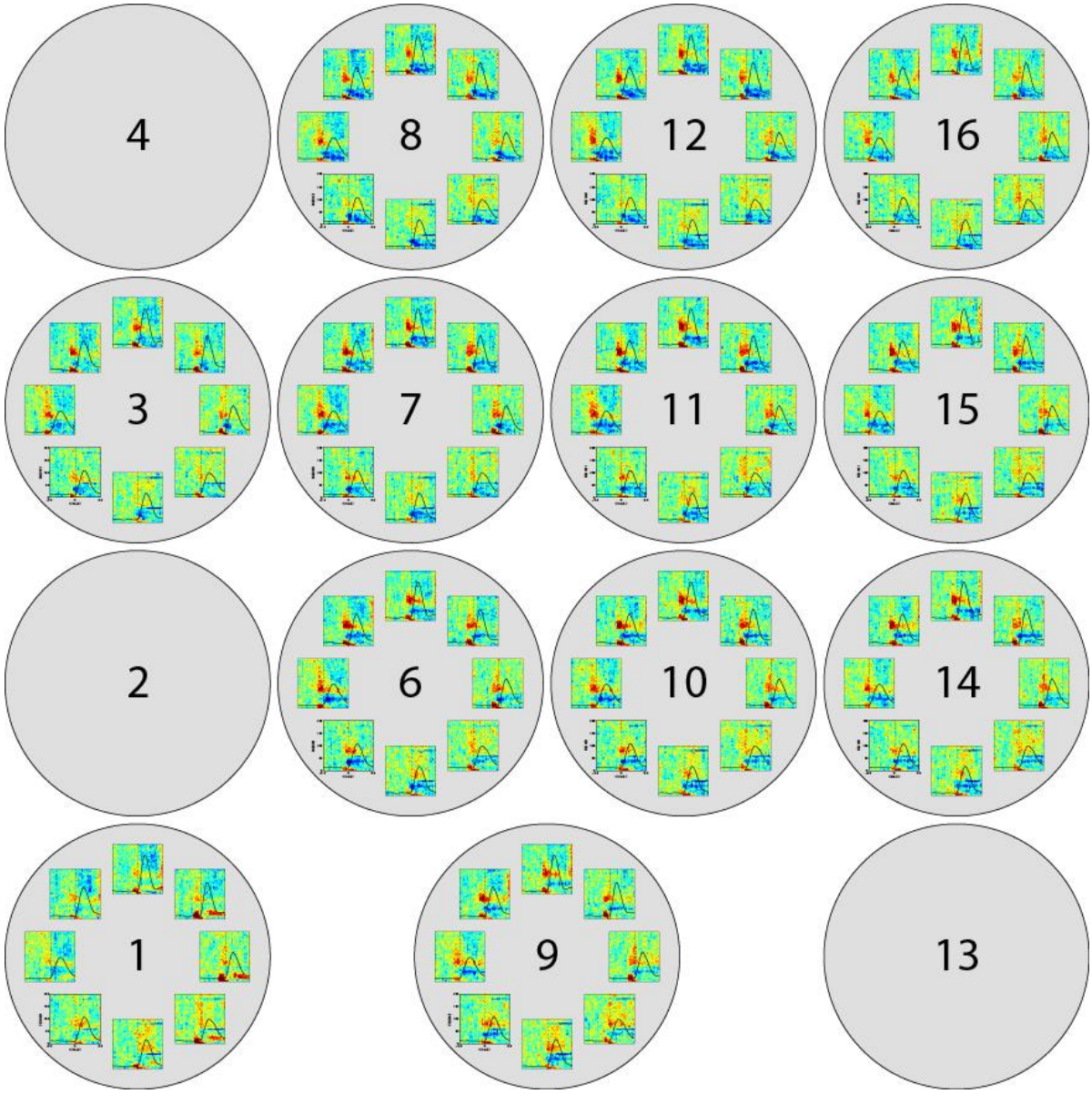

Supplemental Figure B1. Directional modulation of ECoG signals during reaching. Data are shown for all successful reaching trials (N = 1,145). Movement onset is indicated by the dashed black line for each plot. Data for electrodes 4 and 13 are not available on account of these electrodes serving as ground and reference electrodes, respectively. Data for electrode 2 is not available on account of connectivity of this electrode being lost shortly after grid implantation.

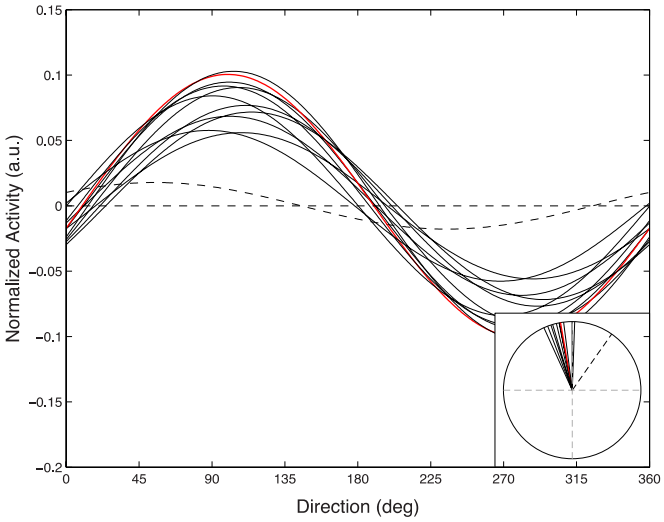

Supplemental Figure B2. Cosine tuning of ECoG signals during reaching. The tuning curve for electrode e10 is shown in red; all other tuning curves are shown in black. Solid lines indicate electrodes exhibiting significant tuning to target direction ($p < 0.05$), while dashed lines indicate non-significant fits. *Inset*: Normalized preferred directions for each channel plotted on a unit circle. The mean of each curve (b_0) has been removed prior to plotting.

Supplemental Section C: Longitudinal Impedance and RMS Amplitude

C.1. Electrode impedance

Electrode impedances were measured both over the course of electrode implantation (*in vivo*) and after explantation (*ex vivo*). Impedance was measured at 20Hz using the g.USBamp biosignal amplifier (g.tec Medical Engineering). *In vivo* impedance measurements were made for each ECoG grid electrode using the recording ground and reference electrodes (e4 and e13, respectively) shorted together with one of the animal's headposts as the counter electrode. *Ex vivo* impedance was measured for each ECoG grid electrode in saline with two counter electrode configurations: one using the recording ground and reference electrodes (e4 and e13, respectively) shorted together, and one using an external calomel electrode (reference) and platinum foil electrode (ground) shorted together. For both *ex vivo* configurations, impedance was measured with the grid in the encapsulating tissue envelope and after removal from the encapsulation, with the goal of assessing the impedance contribution of the encapsulating tissue. Analysis of impedance measurements were restricted to the mean of 2mm-diameter electrodes which retained electrical connectivity throughout the course of the experiment.

In vivo mean electrode impedance (Supplemental Figure C1A) was found to be relatively stable over the course of the study. However, electrode impedance was observed to decrease following surgical intervention on day 271 post-implantation to repair an acrylic island used to cover the electrode grid wire bundle. The cause of this decrease in impedance is unclear, though it may be the case that this surgical intervention resulted in unintentional movement of the electrode grid relative to the cortex. *Ex vivo* impedance measurements (Supplemental Figure C1B) indicate that the presence of the encapsulation tissue likely increased electrode impedance, as extraction of the electrode grid from the encapsulating tissue drastically reduced measured impedance values. However, *ex vivo* measurements were performed on fixed encapsulation tissue; the actual contribution of the encapsulation to the *in vivo* impedance would most likely be less than the observed values.

D.2. RMS amplitude analysis

In order to assess changes in electrophysiological recordings over the course of the study, mean electrode root-mean-squared (RMS) amplitudes were calculated for selected datasets. For each dataset analyzed, 10-minute long segments at the beginning of the recording session were inspected for the presence of artifacts; these artifacts were excluded from subsequent analyses. ECoG signals were then re-referenced with respect to the common-mode average, notch-filtered to remove power-line contamination, segmented into 1-second epochs, and band-pass filtered in 5Hz frequency bands over the 5Hz-195Hz range using 4^{th}-order Butterworth filters. RMS values were computed for the resultant band-pass-filtered segments for each frequency band.

Mean electrode RMS amplitudes of recorded ECoG signals were found to decrease over the course of the study (Supplemental Figure C1C, D), appearing to stabilize approximately 300 days post-implantation. The gradual decrease in signal amplitude observed is consistent with the development of encapsulation tissue over time. This development would increase the distance between the electrodes and cortex, which based on volume conductor models would be expected to reduce measured electrical potentials (Rattay 1988).

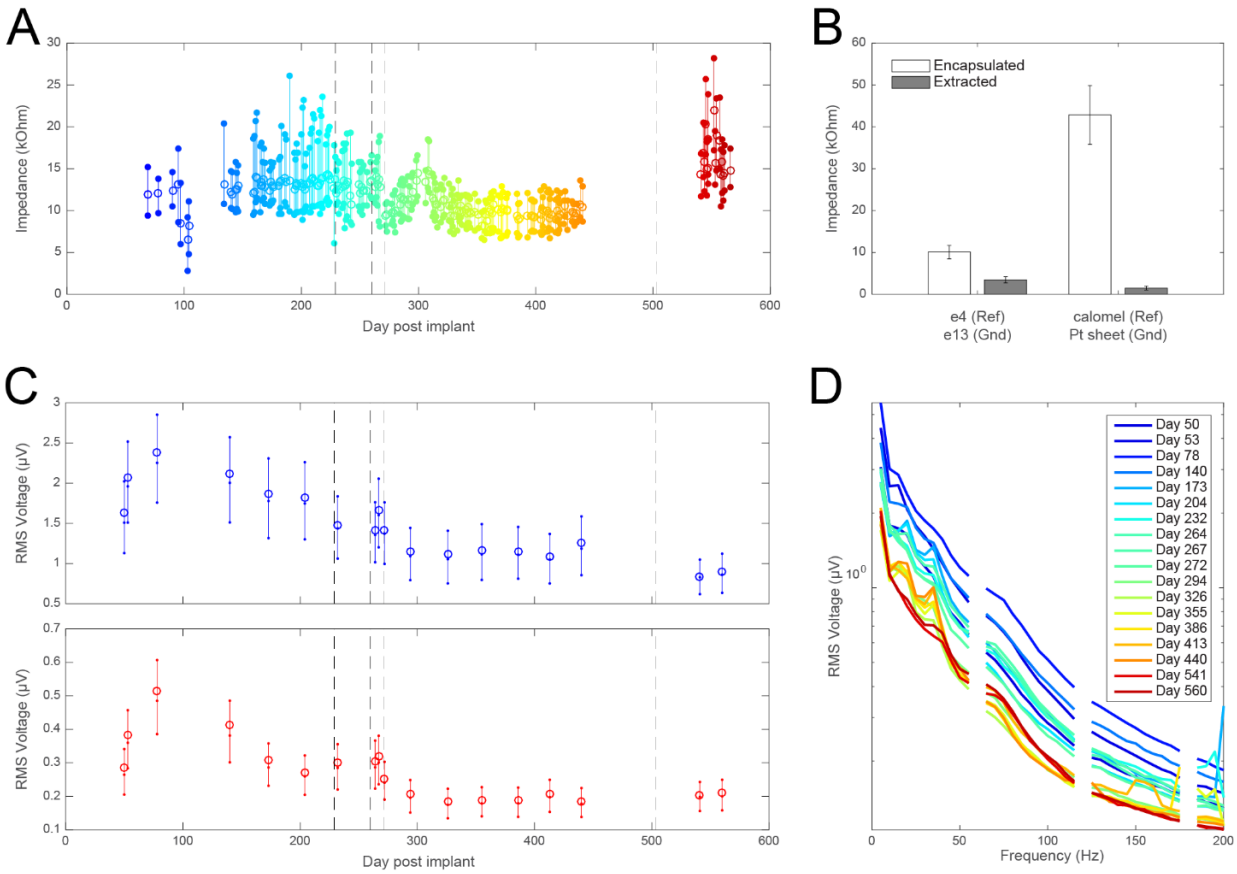

Supplemental Figure C1. Electrode impedance and RMS amplitude of electrophysiological recordings. (A). *In vivo* electrode impedance values (measured at 20Hz) over the course of electrode grid implantation. For each day impedance was measured, the range of impedance values is indicated by colored vertical lines, while the mean impedance is indicated by open circles. Dashed black lines indicate days on which surgical interventions were performed. (B). *Ex vivo* electrode impedance values. Impedance data are shown for both 'e4 + e13' and 'calomel + Pt' measurement configurations (see supplemental methods) for the electrode grid during encapsulated (white) and extracted (gray) conditions. Error bars indicate standard deviations from the mean impedance values for each condition. (C). RMS amplitude over the course of electrode implantation. RMS amplitude at 20Hz (blue) and 100Hz (red) is shown for selected recording sessions. Solid vertical lines indicate the [25th – 75th] quantile range of RMS amplitudes, with filled circles indicating the 25th, 50th, and 75th quantile values. Open circles indicate the mean RMS amplitude. (D). RMS amplitude spectra for selected recording sessions. Mean RMS spectra are provided for the same recording days shown in (C). Individual spectra colors correspond to those of the *in-vivo* impedance data in (A).

Supplementary References

Georgopoulos, A. P., Kalaska, J. F., Caminiti, R., & Massey, J. T. (1982). On the relations between the direction of two-dimensional arm movements and cell discharge in primate motor cortex. *The Journal of Neuroscience: the Official Journal of the Society for Neuroscience*, *2*(11), 1527–1537.

(Ratlay, 1988) Rattay, F. (1988). Modeling the excitation of fibers under surface electrodes. IEEE Transactions on Bio-Medical Engineering, 35(3), 199–202. http://doi.org/10.1109/10.1362